This is the accepted manuscript made available via CHORUS. The article has been published as:

Qubit-Based Memcapacitors and Meminductors

Sergey N. Shevchenko, Yuriy V. Pershin, and Franco Nori

Phys. Rev. Applied **6**, 014006 — Published 14 July 2016

DOI: 10.1103/PhysRevApplied.6.014006

Qubit-based memcapacitors and meminductors

Sergey N. Shevchenko,[1,2,3] Yuriy V. Pershin,[4,3,5] and Franco Nori[3,6]

[1]*B. Verkin Institute for Low Temperature Physics and Engineering, Kharkov 61103, Ukraine*
[2]*V. Karazin Kharkov National University, Kharkov 61022, Ukraine*
[3]*CEMS, RIKEN, Saitama 351-0198, Japan*
[4]*Department of Physics and Astronomy and Smart State Center for Experimental Nanoscale Physics, University of South Carolina, Columbia, South Carolina 29208, USA*
[5]*Nikolaev Institute of Inorganic Chemistry SB RAS, Novosibirsk 630090, Russia*
[6]*Physics Department, University of Michigan, Ann Arbor, Michigan 48109-1040, USA*

It is shown that superconducting charge and flux quantum bits (qubits) can be classified as memory capacitive and inductive systems, respectively. We demonstrate that such memcapacitive and meminductive devices offer remarkable and rich response functionalities. In particular, when subjected to periodic input, qubit-based memcapacitors and meminductors exhibit unusual hysteresis curves. Our work not only extends the set of known memcapacitive and meminductive systems to qubit-based devices but also highlights their unique properties potentially useful for future technological applications.

I. INTRODUCTION

There has recently been drastically increasing interest in electronic circuit elements with memory, namely, memristive [1,2], memcapacitive and meminductive [3] systems (for a recent review see Ref. [4]). In these resistive, capacitive and inductive devices, the instantaneous response depends on the history of the signals applied. While prominence has been given to memristive devices, memcapacitive and (less frequently) meminductive devices are also investigated. However, with few rare exceptions [5–7], attention has been focused on devices operating in the *classical* regime. Therefore, it is intriguing to find *quantum* realizations, especially of memcapacitive and meminductive systems, since these are not currently known.

In this regard, superconducting devices [8] are attractive from several points of view. First of all, the past decade has witnessed great progress in the area of superconducting qubits [9–11], which operate in the quantum regime. Second, the relevance of *classical* superconducting devices to the area of memory circuit elements has already been established. Examples include: (*i*) phase-dependent conductance, interpreted as memristive phenomenon [12,13]; (*ii*) the voltage-history dependence of the inductance (for more information on this meminductance, see Appendix A and Ref. [12]); (*iii*) various hystereses in different settings, such as, for example, the average voltage-current hysteresis in the CRSJ model [8,14], which can be interpreted as a memristive phenomenon. In Appendix A, the meminductance of the Josephson junction is considered in detail to better explain some novel aspects of the Josephson effect.

Surprisingly, it is not necessary to look very far to find examples of *quantum* superconducting memory devices. Indeed, the natural candidate (a superconducting qubit [9–11]) is a quantum two-level system that, depending on the setting, offers a memcapacitive or meminductive response. The goal of the present paper[38] is to demonstrate the correspondence between superconducting qubits and memory circuit elements. An interesting distinctive feature of these quantum memory devices (compared to the traditional ones such as considered in Ref. [15]) is their rich internal dynamics, stemming from the quantum internal dynamics of qubits. In the past, many of such dynamical properties were demonstrated experimentally, including coherent Rabi oscillations, Landau-Zener tunneling, etc. [9–11,16] We emphasize that while we consider superconducting qubits, our approach can be extended to other types of qubits.

Mathematically, memory circuit elements are defined by [3]

$$y(t) = g(\mathbf{x}, u, t)u(t), \tag{1}$$
$$\dot{\mathbf{x}} = \mathbf{f}(\mathbf{x}, u, t). \tag{2}$$

Here, $u(t)$ and $y(t)$ are complementary constitutive circuit variables denoting the input and the output of the system, g is the generalized response function, $\mathbf{x}$ is the set of variables describing the internal state, and $\mathbf{f}$ is the vector function defining the evolution of $\mathbf{x}$.

To be more specific, voltage-controlled memcapacitive systems [3] are described by

$$Q(t) = C_{\rm M}(\mathbf{x}, V, t)V(t), \tag{3}$$
$$\dot{\mathbf{x}} = \mathbf{f}(\mathbf{x}, V, t), \tag{4}$$

where the memcapacitance $C_{\rm M}$ is given by the relation between the charge Q and voltage V. Current-controlled meminductive systems [3] are given by

$$\phi(t) = L_{\rm M}(\mathbf{x}, I, t)I(t), \tag{5}$$
$$\dot{\mathbf{x}} = \mathbf{f}(\mathbf{x}, I, t), \tag{6}$$

where the meminductance $L_{\rm M}$ defines the relation between the flux-linkage $\phi \equiv \int V{\rm d}t$ and the current I. We note that Eqs. (3-4) and (5-6) are particular cases of Eqs. (1-2).

In what follows, we show that the above equations match the equations for certain expectation values calculated for qubit-based memcapacitors and meminductors.

In other words, the suggested devices behave *on average* as classical memcapacitors and meminductors in some simple circuits studied in this work. In what follows, such quantum-mechanically averaged values are denoted with angular brackets. At the same time, the individual measurements of the output of our devices will exhibit quantum uncertainty. This uncertainty is a clear manifestation of the non-classical (quantum) nature of our devices. This issue is also addressed in Ref. [17], where a driven quantum system is described by the respective average voltages and currents, of which the relation is studied for the description of the quantum memristor operation. Additionally, in more complex circuits than the ones considered here, several qubit-based devices may form various non-trivial quantum states (such as, e.g., entangled states) that would require a quantum approach to describe the circuit dynamics. In any case, in this work the qubit-based memcapacitors and meminductors are considered as quantum systems capable to store quantum information.

This paper is organized as follows. In Sec. II, we present descriptions of charge and flux qubits as memory circuit elements, showing that their electrical response can be formulated in the form of Eqs. (3) and (5), respectively. Then, in Sec. III, we discuss the dynamics of the internal state variables of qubits. We show that the equations of motion for the internal state variables can be written in the form of Eqs. (4, 6). Simulation results are described in Sec. IV, which presents various types of hysteretic loops. Finally, we conclude in Sec. V. Details of calculations are presented in the Appendices. Moreover, the quantum uncertainty of measurements is discussed in the last Appendix.

II. QUBITS AS MEMORY DEVICES

We will focus on charge and flux qubits, showing that they belong to the general classes of memcapacitive and meminductive systems. For this purpose, we cast the qubit equations in the form of Eqs. (3-4) and (5-6), respectively, thus identifying the internal state variables, response and evolution functions. It is interesting that the equations for charge and flux qubits can be written exactly in the same form, when we treat these structures as memory circuit elements. The circuit elements and notations are summarized in Fig. 1 and Table I.

Below, we use a semiclassical approach, where the quantum-mechanical evolution of the qubit is considered in the presence of the classical input $u(t)$. The system output $y(t)$ is calculated as an expectation value. Such model assumes the input and output to be described by coherent states, involving many photons. For more details on the semiclassical approximation, see, e.g., Ref. [18].

In what follows, we consider both the case when the dissipative environment can be disregarded (good isolation; the system can be described by the Liouville equation), and also the case with significant dissipation (which is introduced phenomenologically and may include the effect of the measurement apparatus; in this case, the system is described using the dissipative Bloch equation). The Bloch equation includes the effect of non-zero temperature T as well as the relaxation and decoherence rates, Γ_1 and Γ_2. We note that neglecting these rates, $\Gamma_1 = \Gamma_2 = 0$, reduces the Bloch equation to the Liouville equation.

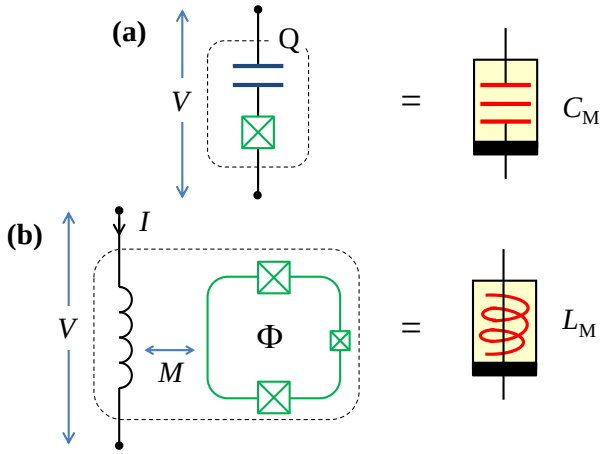

FIG. 1: Superconducting qubits as memory circuit elements. (a) The charge qubit implements a memcapacitive system. (b) A coil inductively coupled to a flux qubit forms an effective meminductive system. The crossed boxes denote Josephson junctions, the circuit symbols of memcapacitor (top) and meminductor (bottom) are shown on the right.

A. Charge qubit

Consider first the superconducting charge qubit, Fig. 1(a). Its main part, the so-called Copper-pair box, is formed by a gate capacitor C_g and a Josephson junction with a capacitance C_J. The superconducting island

TABLE I: Charge and flux qubits as memcapacitive and meminductive systems.

	Charge qubit	Flux qubit
$u(t)$	$V(t)$	$I(t)$
$y(t)$	Q	$\phi = \int V \mathrm{d}t$
g	$C_M = C_{geom} - \frac{eC_g}{VC_\Sigma}\langle\sigma_z\rangle$	$L_M = L - \frac{MI_p}{I}\langle\sigma_z\rangle$
$\mathbf{x}$	$(X, Y, Z)^\top$	$(X, Y, Z)^\top$
f	$\mathbf{B}\times\mathbf{x} - \Gamma(\mathbf{x} - \mathbf{x}_0)$	$\mathbf{B}\times\mathbf{x} - \Gamma(\mathbf{x} - \mathbf{x}_0)$
Type	Memcapacitive system	Meminductive system

between these two capacitors has the total capacitance $C_\Sigma = C_g + C_J$, and is characterized by the average charge $-2e\langle n\rangle$, where $-e$ is the electron charge and $\langle n\rangle$ is the number of Copper pairs on the island. The island is assumed to be biased by a voltage, which, in general, contains both time-dependent, $V(t)$, and dc, V_{dc}, components. From electrostatic considerations, one finds the charge on the external plate of the gate capacitor

$$Q(t) = \frac{C_g C_J}{C_\Sigma}\left[V(t) + V_{dc}\right] - \frac{C_g}{C_\Sigma} 2e\langle n\rangle . \qquad (7)$$

In the two-level approximation [19–21], the charge qubit Hamiltonian is written as

$$H = -\frac{\Delta}{2}\sigma_x - \frac{\varepsilon}{2}\sigma_z, \quad \varepsilon = \varepsilon_0 + \varepsilon_1(t), \qquad (8)$$

where the energy bias $\varepsilon = E_C(2n_g - 1)$ is defined by the island charging energy $E_C = (2e)^2/2C_\Sigma$ and the dimensionless gate voltage $n_g = C_g V/2e$. The tunneling amplitude $\Delta = E_J$ is given by the Josephson energy of the contact, and the σ_i stand for the Pauli matrices in the charge representation. Using $n = (1+\sigma_z)/2$ for the charge operator, Eq. (7) can be written in the form[39]

$$Q = C_{geom} V - \frac{eC_g}{C_\Sigma}\langle\sigma_z\rangle \equiv C_M(\mathbf{x}, V)V, \qquad (9)$$

where $C_{geom} = C_g C_J/C_\Sigma$, and $\mathbf{x}$ stands for the set of parameters describing the time evolution of the charge in the Cooper-pair box [through the $\langle\sigma_z\rangle$ term]. In Eq. (9), for the sake of clarity, we have eliminated the time-independent terms, by choosing the dc bias such that $C_J V_{dc}/e = 1$. Clearly, Eq. (9) is equivalent with Eq. (3). In this way, the charge qubit can be considered as a *memcapacitive* system.

Assuming a periodic input signal of amplitude V_A, Eq. (9) can be presented in the dimensionless form as

$$\frac{Q(t)}{C_{geom} V_A} = \frac{V(t)}{V_A} - \frac{e}{C_J V_A}\langle\sigma_z\rangle . \qquad (10)$$

In particular, taking $V(t) = V_A \sin\omega t$, one can find $\varepsilon_1(t) = A\sin\omega t$, where $A = 2eC_g V_A/C_\Sigma$.

B. Flux qubit

Next, we consider the flux qubit coupled via the mutual inductance M to the inductor L biased by the current I, Fig. 1(b). In this arrangement, the electrical response of the coil depends on the qubit state. As the qubit state has a memory on the history of signals applied (to the coil), it is natural to describe the entire system as an inductor with memory, namely, a *meminductive* system [3] operating in the quantum regime. Previously, it was demonstrated [5] that an RCL contour inductively coupled to an inductor represents a classical meminductive system.

The flux qubit is a superconducting ring with three Josephson junctions [9,22]. The two qubit states correspond to persistent currents in the ring in the clockwise and counterclockwise directions. The persistent current amplitude is I_p. The ring is pierced by a magnetic flux Φ with both ac, Φ_{ac}, and dc, Φ_{dc}, components. The former is introduced by the ac current in the inductor L, and the latter can be created by the dc current in the same or in a separate inductor. In the two-level approximation [9,22], the flux qubit is also described by the Hamiltonian (8), where now the parameters have the following meaning: Δ is the tunneling amplitude, σ_i are the Pauli matrices in the flux representation, $\varepsilon_{0(1)} = 2I_p\Phi_0 f_{dc(ac)}$ is the constant (time-dependent) part of the bias defined by the dc (ac) component of the magnetic flux through the qubit loop, $\Phi_0 = h/(2e)$ is the magnetic flux quantum, $f_{dc} = \Phi_{dc}/\Phi_0 - 1/2$, and $f_{ac} = MI(t)/\Phi_0$.

The electromotive force in the coil is given by $\mathcal{E} = -\dot{\Phi}_c - \dot{\Phi}_q$, where Φ_c and Φ_q are the magnetic fluxes through the inductor L due to the current I in the coil and due to the qubit's current I_q, respectively. This can be rewritten for the voltage across the coil

$$V = L\dot{I} + M\dot{I}_q. \qquad (11)$$

Integrating Eq. (11) over time and using $I_q = -I_p\langle\sigma_z\rangle$ one obtains the expression for the flux-linkage ϕ in the form of Eq. (5)

$$\phi = LI - MI_p\langle\sigma_z\rangle \equiv L_M(\mathbf{x}, I)I. \qquad (12)$$

We note that Eq. (12) also nominally coincides with Eq. (9) (see also the generalized notations in the Table I). In Eq. (12), the vector $\mathbf{x}$ stands for a set of parameters defining the qubit state through $\langle\sigma_z\rangle$.

Finally, let us assume that the ac component of the current is $I_A \sin\omega t$. Then, $f_{ac}(t) = MI_A\sin\omega t/\Phi_0$, so that $\varepsilon_1(t) = A\sin\omega t$ with $A = 2MI_pI_A$. In the dimensionless form, Eq. (12) can be written as

$$\frac{\phi(t)}{LI_A} = \frac{I(t)}{I_A} - \frac{MI_p}{LI_A}\langle\sigma_z\rangle . \qquad (13)$$

III. DYNAMICS OF THE INTERNAL STATE VARIABLES

In the previous section we obtained relations for the memcapacitance and meminductance, Eqs. (9) and (12), in the form of Eq. (1) with $g(\mathbf{x}, u, t)$ defined by $\langle\sigma_z\rangle$. The dimensionless forms of these expressions, Eqs. (10) and (13), can be written in a unified form

$$\frac{y(t)}{y_0} = \frac{u(t)}{u_0} - \varkappa\langle\sigma_z\rangle , \qquad (14)$$

where, comparing with Eqs. (10) and (13), one can easlily identify y_0, u_0, and $\varkappa$ for the respective two cases. Let us now clarify what are the variables that form the vector $\mathbf{x}$ and define $\langle\sigma_z\rangle$.

Previously, the Hamiltonians and Pauli matrices σ_i were defined in the physical bases, which are the charge basis for the charge qubit and the current basis for the flux qubit. In these bases, $\langle\sigma_z\rangle$ provides the difference between the probabilities of the two charge states and of the two current directions for the charge and flux qubits, respectively. In order to describe the quantum dynamics of a qubit, one has to take into account the dissipative processes. This can be done in the framework of the Bloch equation [9,22,23]. Since the Bloch equation defines the relaxation in the energy representation, one has to change to this basis (see Appendix B for more details).

Let the qubit density matrix in the energy representation be parameterized as $\rho = \frac{1}{2}(1 + \mathbf{x}\sigma)$ with $\mathbf{x} = (X, Y, Z)^\top$ being the so-called Bloch vector. The Bloch vector thus plays the role of the *internal state variables* of qubits. Changing from the physical representation to the energy one, we obtain

$$\langle\sigma_z\rangle = -\frac{\Delta}{\Delta E}X + \frac{\varepsilon_0}{\Delta E}Z, \tag{15}$$

with $\Delta E \equiv \hbar\omega_{\rm q} = \sqrt{\Delta^2 + \varepsilon_0^2}$. Equation (15) describes how the response function g in Eqs. (9) and (12) depends on the components of the Bloch vector $\mathbf{x}$. Moreover, for the sake of simplicity, we assume that the two phenomenological relaxation rates entering the Bloch equation are the same (see Appendix B), namely, $\Gamma_2 = \Gamma_1 \equiv \Gamma$. In this way, one can write the Bloch equation as

$$\dot{\mathbf{x}} = \mathbf{f}(\mathbf{x}, u) \equiv \mathbf{B} \times \mathbf{x} - \Gamma(\mathbf{x} - \mathbf{x}_0), \tag{16}$$

where

$$\mathbf{B} = (B_x, 0, B_z)^\top, \quad \mathbf{x}_0 = (0, 0, Z_0)^\top, \tag{17}$$

$$B_x = \frac{\Delta}{\Delta E}\frac{\varepsilon_1(t)}{\hbar} \equiv 2\Omega_{\rm R}^{(0)} \sin\omega t, \tag{18}$$

$$B_z = -\omega_{\rm q} - \frac{\varepsilon_0}{\Delta}B_x, \quad \Omega_{\rm R}^{(0)} = \frac{\Delta A}{2\hbar\Delta E}, \tag{19}$$

and $Z_0 = \tanh(\Delta E/2k_{\rm B}T)$ describes the equilibrium energy level populations.

Equation (16) corresponds to the generic equation (2) and, together with Eqs. (9) and (12) [which are in the form of Eq. (1)], completes the model of qubit-based systems as realizations of memory circuit elements.

IV. ILLUSTRATIVE EXAMPLES

Frequency-dependent pinched hysteresis loops are the most pronounced signatures of memory circuit elements [2–4]. In this section we consider qubit-based memcapacitors and meminductors subjected to a periodic input, $\varepsilon_1(t) \propto u(t) = u_0 \sin\omega t$. The examples presented below highlight the unusual dynamical features of these quantum devices.

We emphasize that Figs. 2-4 illustrate hysteresis curves for both charge and flux qubits. For the charge qubit: $u = V$, $u_0 = V_{\rm A}$, $y = Q$, and $y_0 = C_{\rm geom}V_{\rm A}$. For the flux qubit: $u = I$, $u_0 = I_{\rm A}$, $y = \phi$, and $y_0 = LI_{\rm A}$.

A. Rabi oscillations

Consider the situation when the applied frequency is close to the resonance frequency, so that $\delta\omega \equiv \omega - \omega_{\rm q} \ll \omega$. If the relaxation time Γ^{-1} is quite long, one can ignore the relaxation and find an analytical solution for the problem (see Appendix B for details). In particular, precisely at the resonance ($\omega = \omega_{\rm q}$), we obtain:

$$\langle\sigma_z\rangle = \frac{\varepsilon_0}{\Delta E}\cos\Omega_{\rm R}^{(0)}t - \frac{\Delta}{\Delta E}\sin\Omega_{\rm R}^{(0)}t\cos\omega t, \tag{20}$$

where $\Omega_{\rm R}^{(0)}$ is given by Eq. (19). Equation (20), describing the Rabi oscillations, can be further simplified, at both the avoided-level crossing and far from this point:

$$\varepsilon_0 = 0: \qquad \langle\sigma_z\rangle = -\sin\Omega_{\rm R}^{(0)}t\cos\omega t, \tag{21}$$

$$|\varepsilon_0| \gg \Delta: \qquad \langle\sigma_z\rangle = \mathrm{sign}(\varepsilon_0)\cos\Omega_{\rm R}^{(0)}t. \tag{22}$$

The case of $\varepsilon_0 = 0$ and $\delta\omega = 0$ corresponds to the excitation by $u(t) = u_0 \sin\omega_{\rm q}t$. Using Eq. (14) we find the system response in this case:

$$\frac{y(t)}{y_0} = \sin\omega t + \varkappa \sin\Omega_{\rm R}^{(0)}t\cos\omega t. \tag{23}$$

The shape of the hysteresis curve (23) is defined by the commensurability of ω and $\Omega_{\rm R}^{(0)}$. In particular, if the ratio of these frequencies is a rational number, $\Omega_{\rm R}^{(0)}/\omega = n/m$ (here, n and m are integers), then the hysteresis curve is a closed loop. One can show that the period of such a loop is $T^* = nT_{\rm R} = mT_\omega$, where $T_{\rm R} = 2\pi/\Omega_{\rm R}^{(0)}$ and $T_\omega = 2\pi/\omega$ are periods of the Rabi oscillations and periodic input, respectively. In the opposite case of an irrational ratio $\Omega_{\rm R}^{(0)}/\omega$, the curve is not closed. Both cases are illustrated in Fig. 2.

We note that Fig. 2 was obtained using Eq. (23) found in the rotating-wave approximation (see Appendix B). However, at high driving amplitudes, the resonant frequency is shifted according to the Bloch-Siegert expression [24–27]. The corrected resonant frequency can be found numerically by solving the Liouville equation. For the selected set of parameter values, an "8-shaped" closed hysteresis loop [as in Fig. 2(a)] is obtained for $\Omega_{\rm R}^{(0)}/\omega = 1.045$, instead of $\Omega_{\rm R}^{(0)}/\omega = 1$ as predicted in the rotating-wave approximation.

An important feature of the qubit-based memory devices is that their characteristic operational frequencies $\omega_{\rm q}$ belong to the gigahertz region. Such frequencies make the devices controllable by microwaves, on short timescales.

B. Two-photon excitation

Next, we consider a different excitation regime, when the driving frequency is at half the qubit frequency,

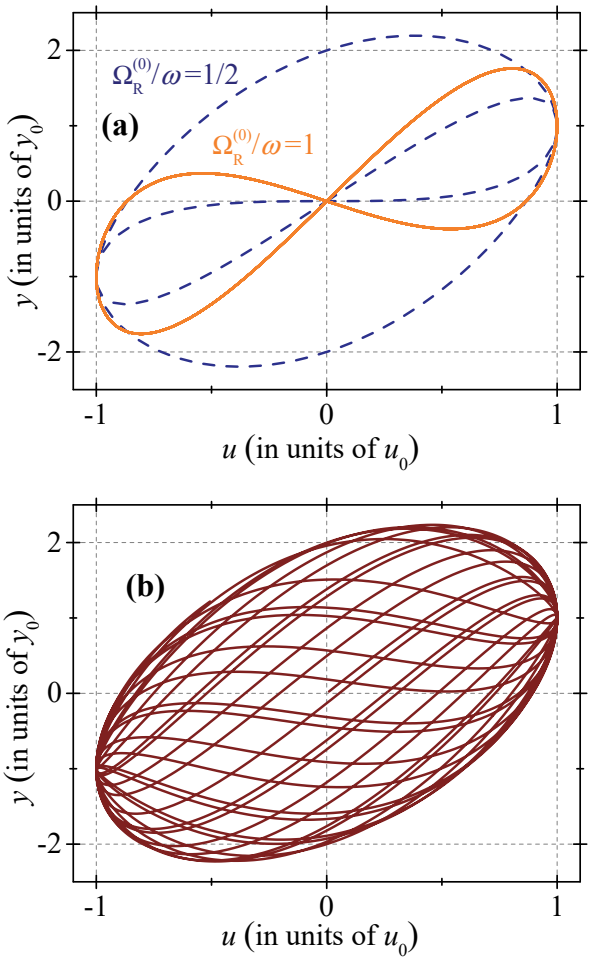

FIG. 2: y versus u hysteresis curves in the Rabi oscillation regime for (a) commensurate and (b) incommensurate frequencies. This plot was obtained using Eq. (23) and the following set of parameter values: $\omega = \omega_q$, $\varkappa = 2$, $\Omega_R^{(0)}/\omega = 1$ (solid curve in (a)), $\Omega_R^{(0)}/\omega = 1/2$ (dashed curve in (a)), $\Omega_R^{(0)}/\omega = 1/\sqrt{2}$ (b). (b) presents the curve corresponding to about 16 periods of the sinusoidal input.

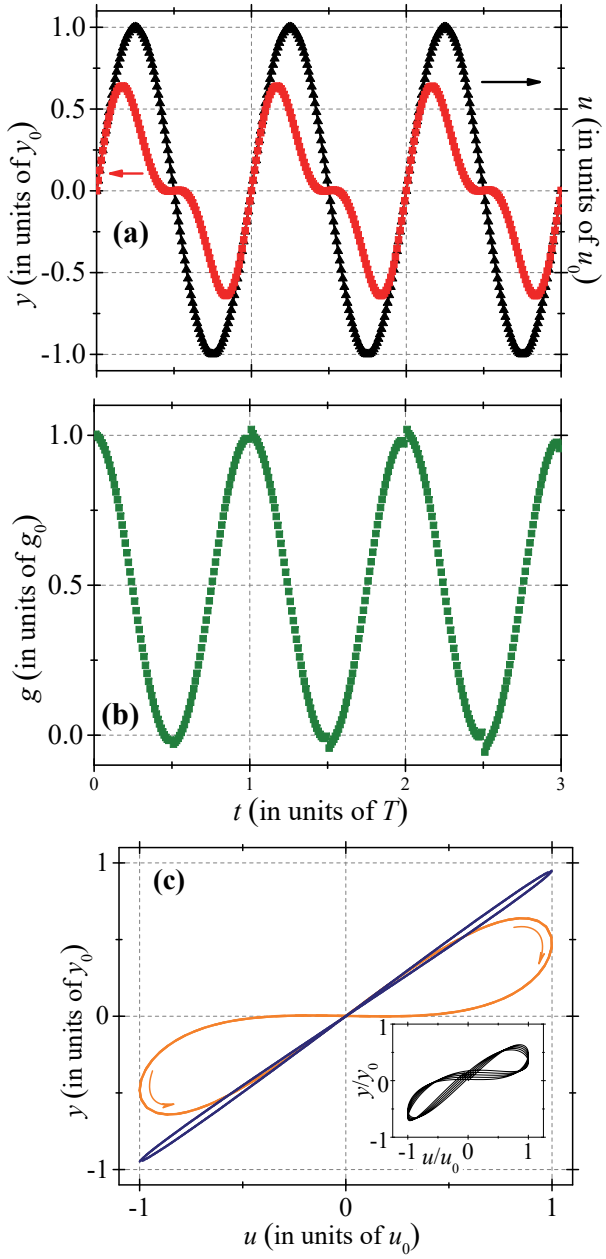

FIG. 3: Time-dependencies of (a) the input u and output y, and (b) the generalized response g for the case of two-photon excitation. (c) y versus u hysteresis curves. These plots were obtained using the following parameter values: $\omega = 1.013 \cdot \omega_q/2$, $\varepsilon_0 = 0$, $\varkappa = 2$, $\Gamma = 0$, and $A = 0.2\Delta$. The narrow hysteresis curve in (c) is found at a different value of $\varkappa = 0.2$. The inset shows the hysteresis curve found at a different value of $\omega = \omega_q/2$. The inset curve corresponds to five periods of the input oscillations.

$\omega = \omega_q/2$. This is the two-photon process [28] as two photons are required to excite the qubit. The two-photon process is characterized by its own Rabi frequency (see Ref. [18] for more details) that, together with the excitation frequency ω (and possibly some other frequencies) defines the system response.

In particular, at zero offset $\varepsilon_0 = 0$, the two-photon Rabi frequency is zero [18]. The excitation at the two-photon resonant frequency accounted for the Bloch-Siegert shift ($\omega = 1.013 \cdot \omega_q/2$) results in a closed "8-shaped" hysteretic curve depicted in Fig. 3(c), demonstrating the periodicity defined by ω. Figure 3(a)-(b) shows the time dependencies of the input, output, and generalized response function (plotted in units of $g_0 = y_0/u_0$) found in the same calculation by solving the Bloch equation. The shift in the excitation frequency from the resonant one introduces a new periodicity in the response, as shown in the inset of Fig. 3(c). The origin of this modification most probably could be related to a shift of the two-photon Rabi frequency from zero.

C. Delayed response

In the previous subsections, we considered the resonant excitations in which the driving frequency is an integer number of the qubit frequency ω_q, and $\varepsilon_0 = 0$. Here, we consider the opposite case, when the excitation frequency is small and far from the resonance. In this situation, the qubit demonstrates a lag, the finite time needed for the qubit to come into equilibrium. Because of large detuning, there are no Rabi oscillations in this regime.

In order to demonstrate the lagging effect, we select the driving frequency ω comparable to the relaxation rate, for which we choose $\Gamma = 0.01\Delta$, and solve the Bloch equations (16) numerically. Figure 4 shows selected results of these calculations. We found that the largest size hysteresis is observed when the input frequency ω is of the order of $\Gamma/2$. This feature was discussed in detail in Refs. [29–33]

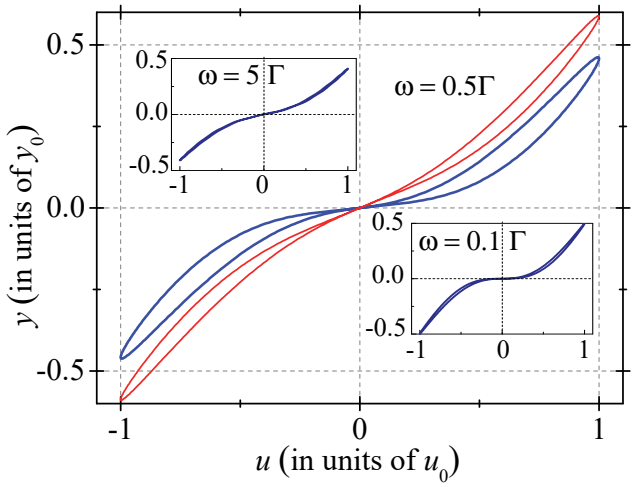

FIG. 4: y versus u hysteretic curves in the delayed response regime. These curves were obtained using the following parameter values: $\Gamma = 0.01\Delta/\hbar$, $A = \Delta$, $\varkappa = 1$, and $\varepsilon_0 = 0$. The values of ω are indicated on the plot. All curves are calculated for zero temperature, except of the thin red curve, which illustrates the effect of the temperature, with $T = 0.5\Delta/k_B$.

The insets in Fig. 4 demonstrate that at lower and higher driving frequencies (compared to Γ) the hysteresis vanishes. Indeed, if the frequency is high, the system does not have enough time to relax to equilibrium. At very low frequencies, the system stays very close to the equilibrium at every instant of time, so that the hysteresis is not observed.

Let us finally discuss the effect of the temperature, which was ignored so far. The temperature enters the Bloch equation through the factor $Z_0 = \tanh(\Delta E/2k_BT)$ as well as through the temperature dependence of the decoherence and relaxation rates. Neglecting the latter, the red thin line in Fig. 4 illustrates that a significant temperature, $T \sim \Delta/k_B$, changes the shape of the curve and reduces the width of the hysteresis loop. At $T \gg \Delta/k_B$, this width tends to zero and the dependence becomes linear. So, in order to ignore the temperature in this context, it should be much smaller than Δ/k_B, which is usually the case in the experimental realizations of qubit-based systems.

D. General picture

In order to better understand the features of the hysteretic response, we plot the hysteresis of X in different cycles of the sinusoidal input calculated as

$$\Delta X_n = X(3T_\omega/8 + nT_\omega) - X(T_\omega/8 + nT_\omega), \qquad (24)$$

where n is the number of the cycle, and $T_\omega = 2\pi/\omega$ is the period of the input signal. Figure 5 presents an example of such calculation. In particular, in Fig. 5(a) at ω/ω_q slightly less than unity, one can clearly recognize the Rabi oscillations corresponding to the solid line in Fig. 2(a). At lower frequencies [see 5(b)] one can distinguish several horizontal lines of a fixed-size hysteresis. These likely correspond to the k-photon processes at $\omega/\omega_q \approx 1/k$, similarly to the two-photon case with $k = 2$ considered above.

Few other plots of hysteresis in X found at different parameter values are provided in Appendix C.

V. CONCLUSION

We demonstrated that several qubit-based structures belong to the class of memory circuit elements [3]. It was shown that when subjected to a periodic input, such qubit-based memcapacitive and meminductive systems exhibit frequency-dependent hysteresis curves. Note that the quantumness of superconducting qubits requires special care in performing and interpreting experiments with such devices. In particular, in addition to the basic components considered in this work, realistic experimental setups include an additional apparatus for measuring the quantum subsystem state. For the sake of simplicity, this issue was not addressed here, since our aim is to demonstrate the aspects of the qubit dynamics relevant to memory devices. Various measurement techniques are discussed, e.g., in Ref. [9].

Our work not only extends the set of memory circuit elements with novel components featuring an unusual and rich quantum dynamics of their internal states, but may also result in novel applications of qubit-based structures beyond the ones traditionally considered for superconducting qubits.

Acknowledgments

S.N.S. is grateful to A. Fedorov, M.F. Gonzalez-Zalba, A.N. Omelyanchouk, and O.G. Turutanov for valuable

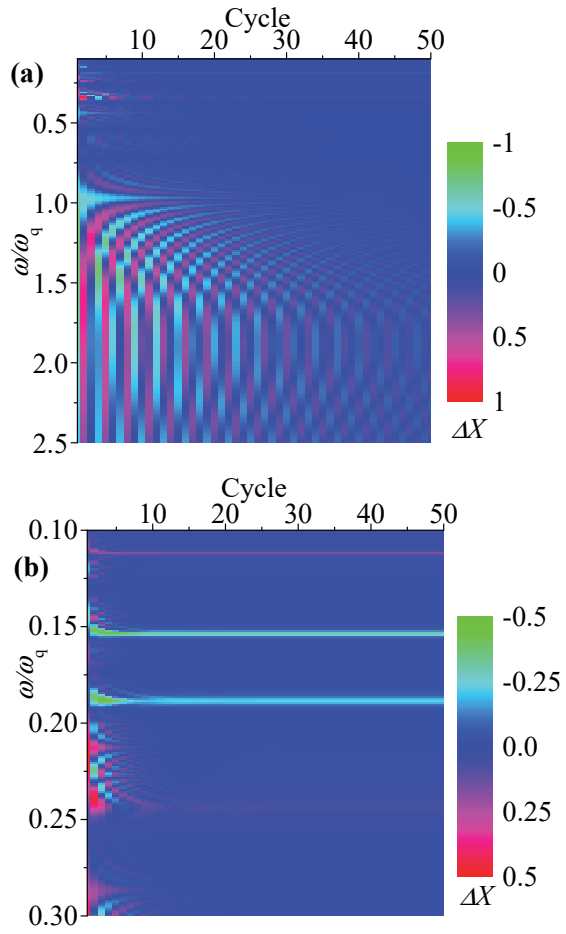

FIG. 5: (a) Hysteresis of X as a function of ω and cycle calculated using Eq. (24). This plot was obtained employing the following set of parameters: $\varepsilon_0 = 0$, $\Omega_{\rm R}^{(0)}/\omega_{\rm q} = 1$, and $\Gamma = 0.01\Delta/\hbar$. (b) Zoom of the low-frequency region in (a).

discussions. This work has been supported by the NSF grant No. ECCS-1202383, USC Smart State Center for Experimental Nanoscale Physics, RIKEN iTHES Project, MURI Center for Dynamic Magneto-Optics, a Grant-in-Aid for Scientific Research (A), a grant from the John Templeton Foundation, the State Fund for Fundamental Research of Ukraine, and the Russian Scientific Foundation grant No. 15-13-20021.

Appendix A: Meminductance of a Josephson junction

Here we present several results which allow interpreting a Josephson junction as a memory device. From the original work by Josephson, it is known that the resistance of the junction contains a phase-dependent term [8,34], which can be treated as a memristance [12]. This was recently studied in Ref. 13. In addition to this, the well-known Josephson inductance can be treated as a meminductance. From this perspective, according to Ref. 12, the correct model for a Josephson junction should include a resistor R, a capacitor $C_{\rm J}$, a memristor $R_{\rm M}$, and a meminductor $L_{\rm J}$, as shown in Fig. 6, left upper inset. These aspects deserve special attention. So, before considering Josephson-junction-based effective two-level systems, qubits, let us describe here the Josephson meminductance. For simplicity, we will not address here neither the phase-dependent memristance, nor other aspects, which result in hysteretic dependencies. Note that the phase-dependent memristance in a related context was studied both in the classical [13] and quantum [17] regimes.

It is known that a Josephson junction can be described as a Josephson inductance. This directly follows from the two Josephson relations, which relate the current I and the voltage V with the order parameter phase difference φ:

$$I(t) = I_{\rm c}\sin\varphi(t), \tag{A1}$$

$$V(t) = \frac{\Phi_0}{2\pi}\dot{\varphi}, \tag{A2}$$

where $I_{\rm c}$ is the critical current of the junction and $\Phi_0 = h/2e$ is the flux quantum. These can be rewritten as

$$V(t) = \frac{\Phi_0}{2\pi\cos\varphi}\dot{I} \equiv L_{\rm J}(\varphi)\dot{I}, \tag{A3}$$

so that the proportionality term is used for the definition of the inductance $L_{\rm J}$. This inductance is often referred to as the *nonlinear inductance*. Strictly speaking, to be nonlinear, this must be a function of the voltage V, namely it must be determined by the instantaneous value of the voltage. Instead, the inductance depends on the phase difference φ, defined by the voltage history. That is why, following Ref. 12, we argue that it would be more correct to call this a *memory inductance*, or meminductance. Indeed, integrating Eq. (A2), one obtains

$$\varphi(t) = \varphi_0 + \frac{\Phi_0}{2\pi}\int_0^t V(t')dt'. \tag{A4}$$

Consequently, the inductance of the Josephson junction $L_{\rm J}(\varphi)$ is precisely the memory inductance, since the phase φ has a memory of the voltages applied in the past.

One can introduce the generalized flux as

$$\Phi = \int_0^t V(t')dt', \tag{A5}$$

which relates it to the phase difference φ in Eq. (A4). Then we can rewrite the above expressions, so that the Josephson junction is obviously a *flux-controlled meminductive system* with the control parameter $x = 2\pi\frac{\Phi}{\Phi_0}$:

$$\dot{I} = L_{\rm J}^{-1}(\Phi)V, \tag{A6}$$

$$\dot{\Phi} = V. \tag{A7}$$

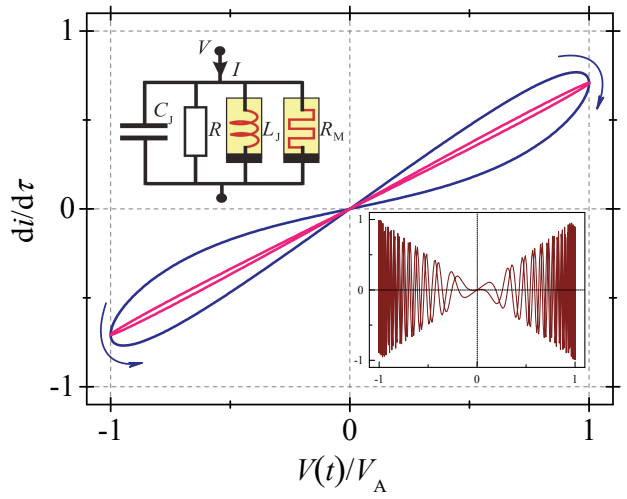

FIG. 6: Josephson junction as a meminductor. Left upper inset: model of a Josephson junction which describes the Josephson inductance $L_{\rm J}$ as the meminductance and also includes the memristance $R_{\rm M}$. Main panel: dependence of the current time-derivative on the applied voltage. The voltage $V(t)$ is normalized by its amplitude $V_{\rm A}$; the dimensionless current is $i = I/I_{\rm c}$ and time $\tau = \frac{2eV_{\rm A}}{\hbar}t$. The thick and thin lines are plotted for $\frac{\hbar\omega}{2eV_{\rm A}} = 2$ and 20, respectively, while the right bottom inset is plotted for this value being 0.01. For all three curves we have taken $\varphi_0 = \pi/4$.

We note that for a non-linear element there are different possibilities to introduce the inductance [8], and equation (A6) is one possibility. For an alternative definition see Eq. (5), which is obtained from Eq. (A6); then $L_{\rm M} = \int \dot{I} L_{\rm J} {\rm d}t/I$.

To further explore these relations, let us now consider a junction biased by the alternating voltage $V(t) = V_{\rm A}\cos\omega t$. In Fig. 6 we plot the dependence of the current derivative on the voltage. This hysteretic dependence was plotted for three values of the frequency. This is shown in the thin-line narrow hysteresis for high frequency; the optimal hysteretic loop for the intermediate case, shown by the thick line; and the complicated hysteretic curve for the low frequency, which is presented in the right bottom inset.

1. Hysteresis in the CRSJ model

Consider now the CRSJ model as described above, but with the resistance R and capacitance $C_{\rm J}$ taken into account explicitly. For definiteness, consider the voltage-biased regime with the applied voltage $V(t) = V_{\rm A}\cos\omega t$. The current is given by the extended version of Eq. (A1),

$$I(t) = I_{\rm c}\sin\varphi(t) + \frac{V(t)}{R} + C_{\rm J}\dot{V}(t), \qquad \text{(A8)}$$

which reflects the Kirchhoff law for the circuit shown in Fig. 6. There, for simplicity, we disregard the memristance, to accentuate on the meminductance. With $\varphi(t)$ given by Eq. (A4), the dimensionless version of Eq. (A8) reads:

$$\frac{di}{d\tau} = \cos\left(\varphi_0 + \frac{\sin w\tau}{w}\right)\cos w\tau - \frac{\Omega}{Q}\sin w\tau - \Omega^2\cos w\tau. \qquad \text{(A9)}$$

Here we introduced the dimensionless values

$$i = \frac{I}{I_{\rm c}},\ \ w = \frac{\hbar\omega}{2eV_{\rm A}},\ \ \tau = \frac{\omega t}{w},\ \ \Omega = \frac{\omega}{\omega_{\rm p}}, \qquad \text{(A10)}$$

with the Josephson plasma frequency $\omega_{\rm p}$ and the quality factor Q defined by the capacitance $C_{\rm J}$ and the resistance R, respectively, as follows

$$\omega_{\rm p}^2 = \frac{2eI_{\rm c}}{\hbar C_{\rm J}} = \frac{2E_{\rm C}E_{\rm J}}{\hbar^2},\ \ Q^2 \equiv \beta = \frac{2e}{\hbar}I_{\rm c}R^2C_{\rm J}. \qquad \text{(A11)}$$

Here the plasma frequency is also expressed with the characteristic charging, $E_{\rm C} = (2e)^2/2C_{\rm J}$, and Josephson, $E_{\rm J} = \hbar I_{\rm c}/2e$, energies of the contact, and β is the Stewart-McCumber parameter.

In Fig. 7 we explore the impact of the resistance R and the capacitance $C_{\rm J}$ on the hysteresis considered previously in Fig. 6; note that Fig. 6 corresponds to $Q \to \infty$ and $\Omega \to 0$. Our numerical calculations demonstrate that there is a pinched hysteresis loop for $Q \gtrsim 100$ and $\Omega \lesssim 0.1$. For realistic junctions, it seems that there is no problem both with the former condition of weak damping ($\beta \gg 1$) and with the latter condition ($\omega \ll \omega_{\rm p}$) of neglecting the displacement current next to the Josephson one [8].

Appendix B: Dynamics of the two-level system

Consider now the dynamics of a two-level system, which we consider here, for clarity, for the meminductive case with the flux qubit. The generalization to other cases, such as the one of the charge qubit, is obvious.

The current in the qubit loop is defined [9,22] by its operator, given by $-I_{\rm p}\sigma_z$. In order to take into account relaxation processes, one has to consider the energy representation. Let the qubit density matrix in this representation be parameterized as follows: $\rho = \frac{1}{2}(1 + \mathbf{x}\sigma)$. Changing from the flux representation to the energy representation is executed by means of the matrix $S = \begin{pmatrix} \cos\zeta/2 & \sin\zeta/2 \\ -\sin\zeta/2 & \cos\zeta/2 \end{pmatrix}$ with $\tan\zeta = -\Delta/\varepsilon_0$. Then the qubit current becomes

$$I_{\rm q} = -I_{\rm p}\langle\sigma_z\rangle = I_{\rm p}\left(\frac{\Delta}{\Delta E}X - \frac{\varepsilon_0}{\Delta E}Z\right). \qquad \text{(B1)}$$

One can see that in the *ground/excited state*, $X = 0$ and $Z = \pm 1$: $I_{\rm q} = \mp I_{\rm p}\frac{\varepsilon_0}{\Delta E}$, with zero current at the avoided level crossing, for $\varepsilon_0 = 0$, and with $I_{\rm q} = \pm I_{\rm p}$ far from it, at $|\varepsilon_0| \gg \Delta$.

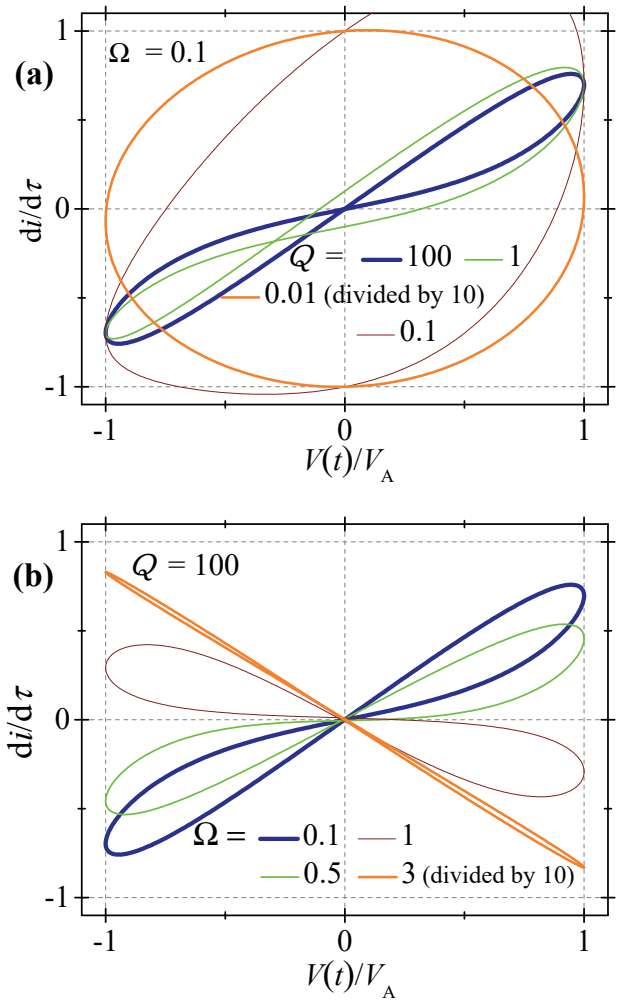

FIG. 7: Impact of the resistance R (upper panel) and capacitance (bottom panel): Dependence of the current time-derivative on the applied voltage. The dimensionless current is $i = I/I_c$ and the reduced time $\tau = \omega t/w$. The parameters used here are: $w = 2$ and $\varphi_0 = \pi/4$; the resistance (i.e., Q) and capacitance (i.e., $\Omega = \omega/\omega_p$) are varied, as shown in the legends.

The qubit current in Eq. (B1) is defined by the difference between the probabilities of the currents in the two directions $\langle\sigma_z\rangle$, which is calculated by solving the Bloch equation [9,22,23]:

$$\begin{aligned}\dot{X} &= -B_z Y - \Gamma_2 X, \qquad \text{(B2)}\\ \dot{Y} &= B_z X - B_x Z - \Gamma_2 Y,\\ \dot{Z} &= B_x Y - \Gamma_1 (Z - Z_0).\end{aligned}$$

Here $\Gamma_{1,2} = T_{1,2}^{-1}$ is the energy and phase relaxation rates, $Z_0 = \tanh(\Delta E/2k_B T)$ corresponds to the equilibrium energy level populations, and

$$B_x = \frac{\Delta}{\Delta E}\frac{\varepsilon_1(t)}{\hbar} \equiv 2\Omega_R^{(0)}\sin\omega t, \quad \Omega_R^{(0)} = \frac{\Delta A}{2\hbar\Delta E}, \qquad \text{(B3)}$$

$$B_z = -\omega_q - \frac{\varepsilon_0}{\Delta}B_x. \qquad \text{(B4)}$$

These equations can also be written in vector form (to better correspond to the theory of memory-devices [3,4]):

$$\dot{\mathbf{x}} = \mathbf{f}(\mathbf{x}, I) \equiv \mathbf{B}\times\mathbf{x} - \Gamma_2\mathbf{x}_\parallel - \Gamma_1(\mathbf{x}_\perp - \mathbf{x}_0), \qquad \text{(B5)}$$

$$\mathbf{x} = \begin{pmatrix} X\\ Y\\ Z\end{pmatrix}, \ \mathbf{B} = \begin{pmatrix} B_x\\ 0\\ B_z\end{pmatrix}, \ \mathbf{x}_0 = \begin{pmatrix} 0\\ 0\\ Z_0\end{pmatrix}, \qquad \text{(B6)}$$

$$B_x(I) = \frac{\Delta}{\Delta E}\frac{2MI_p}{\hbar}I, \ B_z(I) = -\omega_q - \frac{\varepsilon_0}{\Delta E}\frac{2MI_p}{\hbar}I. \qquad \text{(B7)}$$

Here the longitudinal and transversal components of the vector are given by $\mathbf{x}_\parallel = (\mathbf{x}\mathbf{e}_x)\mathbf{e}_x + (\mathbf{x}\mathbf{e}_y)\mathbf{e}_y$ and $\mathbf{x}_\perp = (\mathbf{x}\mathbf{e}_z)\mathbf{e}_z$, respectively. This can be simplified, if $\Gamma_2 = \Gamma_1 \equiv \Gamma$, then Eq. (B5) becomes Eq. (16).

In the case of *free evolution*, when $A = 0$, with long relaxation times, the Bloch equation can be written for the diagonal and off-diagonal density matrix components, respectively $\rho_{00} = \frac{1}{2}(1 + Z)$ and $\rho_{10} = \frac{1}{2}(X + iY)$:

$$\begin{aligned}\dot{\rho}_{10} &= -i\omega_q\rho_{10}, \qquad \text{(B8)}\\ \dot{\rho}_{00} &= 0.\end{aligned}$$

The solution is described by the constant energy-level populations (defined by the initial condition) and the beating, with frequency ω_q, of the off-diagonal components:

$$\begin{aligned}\rho_{00}(t) &= \rho_{00}(0) = \text{const}, \qquad \text{(B9)}\\ \rho_{10}(t) &= \rho_{10}(0)\exp(-i\omega_q t).\end{aligned}$$

Consider now another situation, when the transition between the qubit energy levels is induced by means of the Rabi oscillations under *resonant driving*, when $\delta\omega \equiv \omega - \omega_q \ll \omega$. Then we make the transformation

$$\widetilde{\rho}_{10} = \rho_{10}\exp(i\omega t) \equiv \widetilde{X} + i\widetilde{Y} \qquad \text{(B10)}$$

(the diagonal component Z is left unchanged) and use the rotating-wave approximation (RWA), i.e. neglect the fast-rotating terms, and from (B2) we obtain

$$\begin{aligned}\dot{Z} &= -\Omega_R^{(0)}\widetilde{X} - \Gamma_1(Z - Z_0), \qquad \text{(B11)}\\ \dot{\widetilde{\rho}}_{10} &= (i\delta\omega - \Gamma_2)\widetilde{\rho}_{10} + \frac{1}{2}\Omega_R^{(0)}Z. \qquad \text{(B12)}\end{aligned}$$

The latter equation can be rewritten as:

$$\begin{aligned}\dot{\widetilde{X}} &= -\delta\omega\widetilde{Y} + \Omega_R^{(0)}Z - \Gamma_2\widetilde{X}, \qquad \text{(B13)}\\ \dot{\widetilde{Y}} &= \delta\omega\widetilde{X} - \Gamma_2\widetilde{Y}. \qquad \text{(B14)}\end{aligned}$$

The system of equations (B11, B13, B14) can be solved analytically in two cases: for the stationary case, at times $t \gg T_1, T_2$ and for the case of long relaxation rates, $T_1, T_2 \longrightarrow \infty$. The former solution is obtained by simply

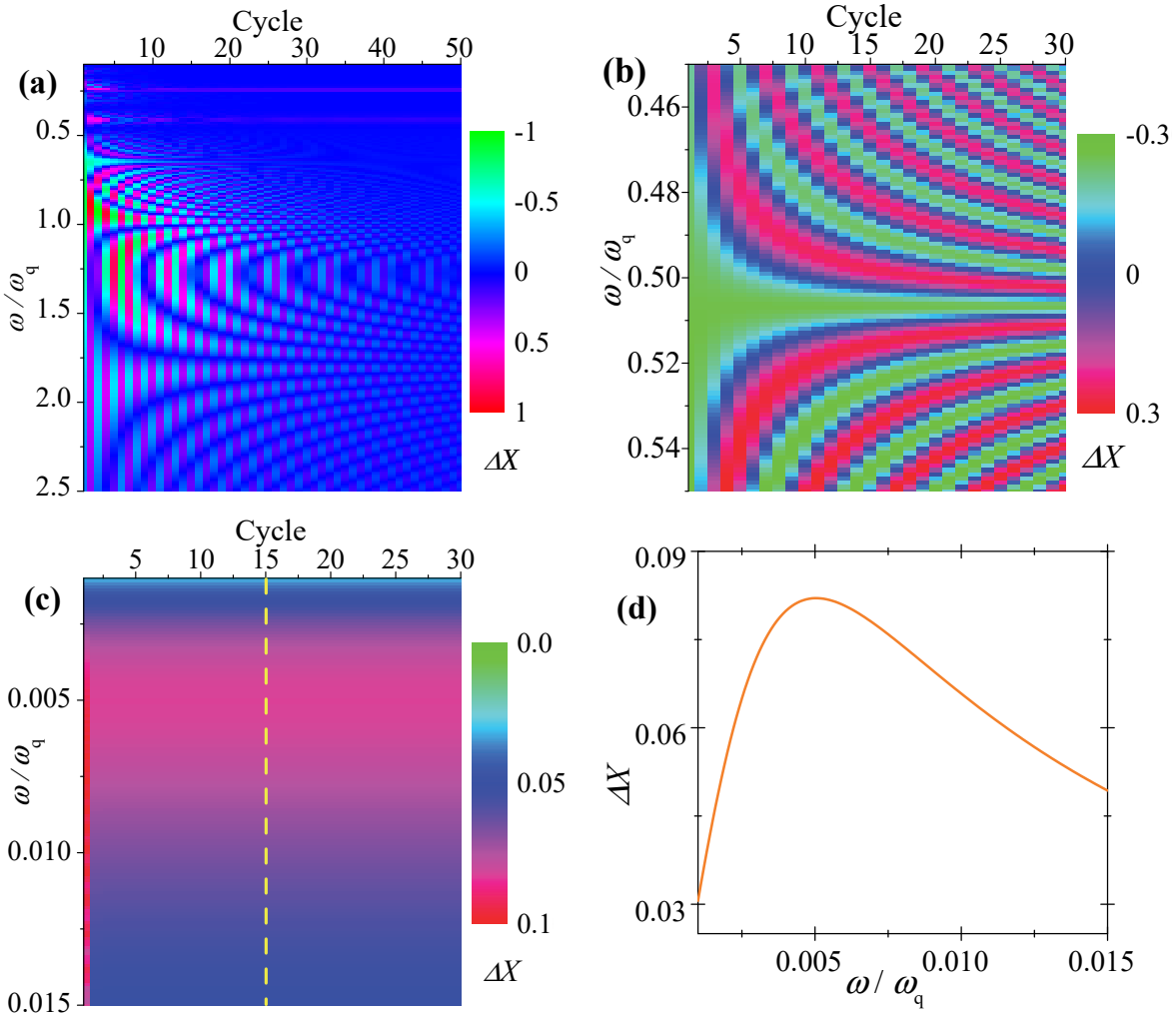

FIG. 8: (a) Hysteresis of X as a function of ω and cycle calculated using Eq. (24). This plot was obtained employing the following set of parameters: $\varepsilon_0 = 0$, $\Omega_{\rm R}^{(0)}/\omega_{\rm q} = 1/2$, $\Gamma = 0.01\Delta/\hbar$. (b) Two-photon excitation regime. The parameter values are similar to the ones in Fig. 3. (c) Hysteresis of X in the delayed-response region found at $\varepsilon_0 = 0$, $\Omega_{\rm R}^{(0)}/\omega_{\rm q} = 1/2$, and $\Gamma = 0.01\Delta/\hbar$. (d) ΔX along the vertical cross-section of (c) denoted by the dashed line.

assuming the l.h.s. of those equations being zero. Consider now in more detail the latter solution to see how Rabi oscillations emerge. In this case we ignore the relaxation terms, and then look for the partial solutions of the differential equations. Let us write down the solutions here for the initial condition of the qubit being in the ground state with $\widetilde{X}(0) = \widetilde{Y}(0) = 0$ and $Z(0) = 1$:

$$\widetilde{X}(t) = \frac{\Omega_{\rm R}^{(0)}}{\Omega_{\rm R}} \sin\Omega_{\rm R} t, \tag{B15}$$

$$\widetilde{Y}(t) = \frac{\delta\omega\Omega_{\rm R}^{(0)}}{\Omega_{\rm R}^2} \left(1 - \cos\Omega_{\rm R} t\right), \tag{B16}$$

$$Z(t) = 1 - \frac{\Omega_{\rm R}^{(0)2}}{\Omega_{\rm R}^2} \left(1 - \cos\Omega_{\rm R} t\right), \tag{B17}$$

$$\Omega_{\rm R} = \sqrt{\Omega_{\rm R}^{(0)2} + \delta\omega^2}. \tag{B18}$$

This provides the formula for the Rabi oscillations (of the upper-level occupation probability):

$$P_+(t) = \frac{1}{2}(1 - Z) = \overline{P_+}\left(1 - \cos\Omega_{\rm R} t\right), \tag{B19}$$

$$\overline{P_+} = \frac{\Omega_{\rm R}^{(0)2}}{2\Omega_{\rm R}^2} = \frac{1}{2}\frac{\Omega_{\rm R}^{(0)2}}{\Omega_{\rm R}^{(0)2} + \delta\omega^2}. \tag{B20}$$

For the qubit current in Eq. (B1), we need Z and X. The former value is given by Eq. (B17) and the latter is found with Eq. (B10):

$$X = \frac{\Omega_{\rm R}^{(0)}}{\Omega_{\rm R}} \left(\sin\Omega_{\rm R} t \cos\omega t + \frac{\delta\omega}{\Omega_{\rm R}} \left(1 - \cos\Omega_{\rm R} t\right) \sin\omega t\right). \tag{B21}$$

In particular, in resonance, at $\delta\omega = 0$ (then $\Omega_{\rm R} = \Omega_{\rm R}^{(0)}$),

we obtain:

$$\frac{I_{\rm q}}{I_{\rm p}} = \frac{\Delta}{\Delta E}\sin\Omega_{\rm R}^{(0)}t\cos\omega t - \frac{\varepsilon_0}{\Delta E}\cos\Omega_{\rm R}^{(0)}t. \qquad \text{(B22)}$$

This is further discussed in the main text, Sec. IV.

Thus we have analyzed the Rabi oscillations. It is worth pointing out that these oscillations can be viewed as a consequence of the constructive interference of the Landau-Zener-Stückelberg-Majorana (LZSM) transitions [16,35]. The opposite case refers to the destructive LZSM interference, which corresponds to the periodic small rising, in the relevant adiabatic basis, of the height given by the LZSM probability. Also we note that besides the sinusoidal driving considered here in detail, there are also other aspects of the qubits driven by different pulses [9], which may also be important in the context of quantum memory devices.

Appendix C: Hysteresis size

In addition to the results presented in Sec. IV, here we provide some additional plots (Fig. 8) that could help to better understand the system's response (in certain ranges of parameters). These plots were obtained similarly to the plots in Fig. 5.

In particular, Fig. 8(a) exemplifies the Rabi oscillations regime (Sec. IV A) for the case of $\Omega_{\rm R}^{(0)}/\omega_{\rm q} = 1/2$. As we previously discussed, for a certain $\omega \sim \omega_{\rm q}$, the period of the hysteresis loop is double the period of the external excitation [see also Fig. 2(a)]. This feature is clearly seen in Fig. 8(a) as an alternation of the hysteresis sign in the consecutive cycles.

Figure 8(b) is related to the two-photon excitation regime (Sec. IV B) showing that a stable hysteresis indeed occurs at a certain $\omega \sim \omega_{\rm q}/2$. The oscillations in the hysteresis appear when ω moves up or down from the hysteretic value. In Fig. 8(c) we additionally explore the delayed-response mechanism of the hysteresis (Sec. IV C). According to Fig. 8(c), the delayed-response mechanism provides a stable hysteresis with a fixed sign. Its maximum corresponds to $\omega \sim \Gamma/2$ as shown in Fig. 8(d).

Appendix D: Quantum uncertainty

Let us finally calculate the quantum uncertainty[36] of the measurement of output. For this purpose, we introduce the output operator $\hat{y}(t)$ as (see Eq. (14))

$$\hat{y}(t) = y_0\frac{u(t)}{u_0} - y_0\varkappa\sigma_z. \qquad \text{(D1)}$$

Then, the standard deviation of y is given by

$$\Delta y(t) = \sqrt{\langle(\hat{y}(t) - y(t))^2\rangle} = \sqrt{\langle\hat{y}^2(t)\rangle - y^2(t)}, \qquad \text{(D2)}$$

where $y(t) = \langle\hat{y}(t)\rangle$. Using Eq. (D1), we finally obtain

$$\Delta y(t) = y_0\varkappa\sqrt{1 - \langle\sigma_z\rangle^2}. \qquad \text{(D3)}$$

Let us illustrate Eq. (D3). For this purpose, we consider the Rabi oscillations example from Sec. IV A. Assuming the case $\varepsilon_0 = 0$ (Eq. (21)) and $\Omega^R/\omega = 1$ (Fig. 2), we get

$$\Delta y(t) = y_0\varkappa\sqrt{1 - \sin^2\Omega_{\rm R}^{(0)}t\cos^2\omega t} \qquad \text{(D4)}$$

that is illustrated in Fig. 9.

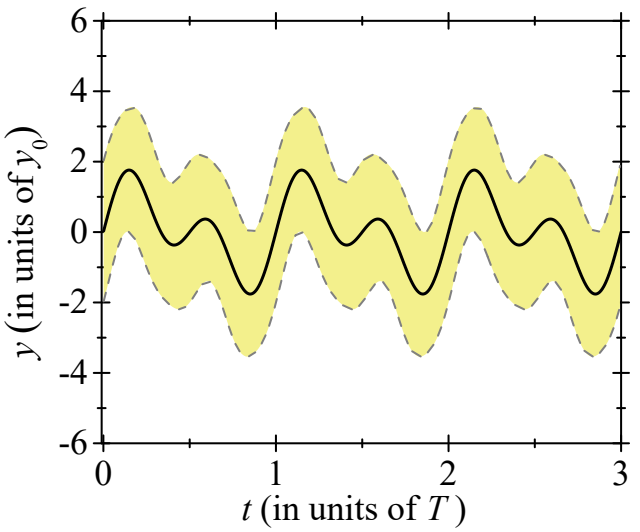

FIG. 9: Time-dependence of the output y and its uncertainty region (the dashed lines represent $y(t) \pm \Delta y(t)$).

[1] L. O. Chua, "Memristor - the missing circuit element," IEEE Trans. Circuit Theory **18**, 507 (1971).

[2] L. O. Chua and S. M. Kang, "Memristive devices and systems," Proc. IEEE **64**, 209 (1976).

[3] M. Di Ventra, Y. V. Pershin, and L. O. Chua, "Circuit elements with memory: Memristors, memcapacitors, and meminductors," Proc. IEEE **97**, 1717 (2009).

[4] Y. V. Pershin and M. Di Ventra, "Memory effects in complex materials and nanoscale systems," Advances in Physics **60**, 145 (2011).

[5] G. Z. Cohen, Y. V. Pershin, and M. Di Ventra, "Lagrange formalism of memory circuit elements: Classical and quan-

tum formulations," Phys. Rev. B **85**, 165428 (2012).
[6] J. E. Gough and G. Zhang, "Classical and quantum stochastic models of resistive and memristive circuits," arXiv:1510.08243 (2015).
[7] P. Pfeiffer, I. L. Egusquiza, M. Di Ventra, M. Sanz, and E. Solano, "Quantum memristors," arXiv:1511.02192 (2015).
[8] K. K. Likharev, *Dynamics of Josephson Junctions and Circuits* (Gordon and Breach, New York, 1986).
[9] G. Wendin and V. S. Shumeiko, "Quantum bits with Josephson junctions," Low Temp. Phys. **33**, 724 (2007).
[10] J. Q. You and F. Nori, "Atomic physics and quantum optics using superconducting circuits," Nature **474**, 589 (2011).
[11] Z.-L. Xiang, S. Ashhab, J. Q. You, and F. Nori, "Hybrid quantum circuits: Superconducting circuits interacting with other quantum systems," Rev. Mod. Phys. **85**, 623 (2013).
[12] L. O. Chua, "Nonlinear circuit foundations for nanodevices, part i: The four-element torus," Proc. IEEE **91**, 1830 (2003).
[13] S. Peotta and M. Di Ventra, "Superconducting memristors," Phys. Rev. Applied **2**, 034011 (2014).
[14] A. Barone and G. Paterno, *Physics and Application of the Josephson Effect* (Wiley, New York, 1982).
[15] J. Martinez-Rincon, Massimiliano Di Ventra, and Yuriy V. Pershin, "Solid-state memcapacitive system with negative and diverging capacitance," Phys. Rev. B **81**, 195430 (2010).
[16] S.N. Shevchenko, S. Ashhab, and F. Nori, "Landau-Zener-Stückelberg interferometry," Phys. Rep. **492**, 1 (2010).
[17] J. Salmilehto, F. Deppe, M. Di Ventra, M. Sanz, and E. Solano, "Quantum memristors with superconducting circuits," arXiv:1603.04487 (2016).
[18] S. N. Shevchenko, G. Oelsner, Ya. S. Greenberg, P. Macha, D. S. Karpov, M. Grajcar, U. Hübner, A. N. Omelyanchouk, and E. Il'ichev, "Amplification and attenuation of a probe signal by doubly dressed states," Phys. Rev. B **89**, 184504 (2014).
[19] M. A. Sillanpää, T. Lehtinen, A. Paila, Y. Makhlin, L. Roschier, and P. J. Hakonen, "Direct observation of Josephson capacitance," Phys. Rev. Lett. **95**, 206806 (2005).
[20] T. Duty, G. Johansson, K. Bladh, D. Gunnarsson, C. Wilson, and P. Delsing, "Observation of quantum capacitance in the Cooper-pair transistor," Phys. Rev. Lett. **95**, 206807 (2005).
[21] G. Johansson, L. Tornberg, V. S. Shumeiko, and G. Wendin, "Readout methods and devices for Josephson-junction-based solid-state qubits," J. Phys. Cond. Matt. **18**, S901 (2006).
[22] Y. Makhlin, G. Schön, and A. Shnirman, "Josephson quantum bits in the flux regime," Physica C **368**, 276 (2002).
[23] K. Blum, *Density Matrix Theory and Applications* (Plenum, New York, 1981).
[24] F. Bloch and A. Siegert, "Magnetic resonance for nonrotating fields," Phys. Rev. **57**, 522 (1940).
[25] S. N. Shevchenko, A. N. Omelyanchouk, A. M. Zagoskin, E. Il'ichev, and F. Nori, "Distinguishing quantum from classical Rabi oscillations in a phase qubit," New J. Phys. **10**, 073026 (2008).
[26] J. Tuorila, M. Silveri, M. Sillanpää, E. Thuneberg, Y. Makhlin, and P. Hakonen, "Stark effect and generalized Bloch-Siegert shift in a strongly driven two-level system," Phys. Rev. Lett. **105**, 257003 (2010).
[27] J. Romhányi, G. Burkard, and A. Pályi, "Subharmonic transitions and Bloch-Siegert shift in electrically driven spin resonance," Phys. Rev. B **92**, 054422 (2015).
[28] S. N. Shevchenko, A. N. Omelyanchouk, and E. Il'ichev, "Multiphoton transitions in Josephson-junction qubits," Low Temp. Phys. **38**, 283 (2012).
[29] M. Grajcar, S. H. W. Van der Ploeg, A. Izmalkov, E. Il'ichev, H.-G. Meyer, A. Fedorov, A. Shnirman, and G. Schön, "Sisyphus cooling and amplification by a superconducting qubit," Nature Phys. **4**, 612 (2008).
[30] F. Nori, "Superconducting qubits: Atomic physics with a circuit," Nature Phys. **4**, 589 (2008).
[31] M. F. Gonzalez-Zalba, S. Barraud, A. J. Ferguson, and A. C. Betz, "Probing the limits of gate-based charge sensing," Nature Comm. **6**, 6084 (2015).
[32] S. N. Shevchenko, D. G. Rubanov, and F. Nori, "Delayed-response quantum back action in nanoelectromechanical systems," Phys. Rev. B **91**, 165422 (2015).
[33] Y. Okazaki, I. Mahboob, K. Onomitsu, S. Sasaki, and H. Yamaguchi, "Gate-controlled electromechanical backaction induced by a quantum dot," Nat. Commun. **7**, 11132 (2016).
[34] B. D. Josephson, "Possible new effects in superconductive tunnelling," Phys. Lett. **1**, 251 (1962).
[35] J. Zhou, P. Huang, Q. Zhang, Z. Wang, T. Tan, X. Xu, F. Shi, X. Rong, S. Ashhab, and J. Du, "Observation of time-domain Rabi oscillations in the Landau-Zener regime with a single electronic spin," Phys. Rev. Lett. **112**, 010503 (2014).
[36] L. D. Landau and L. M. Lifshitz, *Course of Theoretical Physics, Volume III: Quantum Mechanics (Non-Relativistic Theory)*, 3rd ed. (Butterworth-Heinemann, 1981).
[37] Y. V. Pershin, S. N. Shevchenko, and F. Nori, "Memcapacitors and meminductors based on superconducting qubits," in *Proceedings of the International Symposium on Nanoscale Transport and Technology (ISNTT2015), NTT Atsugi R&D Center, Atsugi, Japan, November 17-20* (2015) p. 72.
[38] This paper extends preliminary work reported at the 2015 International Symposium on Nanoscale Transport and Technology (ISNTT2015) [37].
[39] We emphasize that there is a difference between the memcapacitance, defined in Eq. (9), and the effective differential capacitance $C_{\rm eff} = \partial Q/\partial V$ often used in the literature [19–21]. The latter consists of the geometric component $C_{\rm geom}$ and the so-called quantum capacitance $C_{\rm Q} = -\left(C_{\rm g}/C_{\Sigma}\right) 2e\partial \left\langle n \right\rangle /\partial V$.